Resilience assessment of asphalt pavement rutting under climate change

Zhang, Chao; Tan, Yiqiu; Gao, Yangming; Fu, Yongkang; Li, Jilu; Li, Shuai; Zhou, Xingye

DOI
10.1016/j.trd.2022.103395

Publication date
2022

Document Version
Final published version

Published in
Transportation Research Part D: Transport and Environment

Citation (APA)
Zhang, C., Tan, Y., Gao, Y., Fu, Y., Li, J., Li, S., & Zhou, X. (2022). Resilience assessment of asphalt pavement rutting under climate change. *Transportation Research Part D: Transport and Environment*, *109*, Article 103395. https://doi.org/10.1016/j.trd.2022.103395

Transportation Research Part D 109 (2022) 103395

Contents lists available at ScienceDirect

Transportation Research Part D

journal homepage: www.elsevier.com/locate/trd

Resilience assessment of asphalt pavement rutting under climate change

Chao Zhang [a], Yiqiu Tan [a,b,*], Yangming Gao [c], Yongkang Fu [d], Jilu Li [a], Shuai Li [a], Xingye Zhou [e]

[a] School of Transportation Science and Engineering, Harbin Institute of Technology, Harbin 150090, China
[b] State Key Laboratory of Urban Water Resource and Environment, Harbin Institute of Technology, Harbin 150090, China
[c] Faculty of Civil Engineering and Geosciences, Delft University of Technology, Stevinweg 1, 2628 CN Delft, The Netherlands
[d] Poly Changda Overseas Engineering Co., Ltd, Guangzhou 510620, China
[e] Research Institute of Highway, Ministry of Transport, Beijing 100088, China

ARTICLE INFO

Keywords:
Asphalt pavement
Resilience
Climate change
Rutting
Resistance stage
Recovery stage

ABSTRACT

The service performances of asphalt pavement, especially rutting, will be inevitably affected by climate change. However, existing studies have generally focused on the rutting depth and rutting life, and thus became insufficient for comprehensively evaluating the influence of climate change on rutting over the service life. A resilience assessment method for asphalt pavement rutting is developed to solve the above problem. First, the original resilience method is extended to fit the system whose performance level continues to decline. Then, the calculation formulas of rutting resilience are derived by combining the rutting prediction model and the level assessment model. Subsequently, the influence degrees of climate change in representative cities on rutting resilience are studied. The results suggest that neglecting climate change in rutting design of asphalt pavement will lead to insufficient resilience, especially in northern China. Furthermore, the predicted temperature under RCP8.5 should be employed for asphalt pavement design.

1. Introduction

Global warming is one of the main characteristics of future climate change (Li et al., 2022; Tollefson, 2021; Wu et al., 2020). Transportation infrastructures are generally exposed to the natural environments, and the service performances may be affected by climate change (Al Fuhaid et al., 2018; Blaauw et al., 2022; Gao et al., 2022; Gao et al., 2019; Sanchis et al., 2020; Wang et al., 2020b). Asphalt mixture, widely employed for high-grade pavement worldwide, is a typical temperature sensitive material (Chen et al., 2021; Li et al., 2020b; Lu and Harvey, 2011; Wang et al., 2020a; Yu and Lu, 2012; Yu et al., 2018; Zhang et al., 2021b). For the design of asphalt pavement, there is a general assumption that the climate conditions are stable, and the influences of future climate change are not considered (Meagher et al., 2012). The historical climate data over the past three decades are used in China according to the specifications for design of highway asphalt pavement (2017), and the climate data of a certain historical period are used for engineers to select materials according to current standards of roadway design in the United States (Underwood et al., 2017). Using the traditional design methods based on historical meteorological data may lead to wrong selections of asphalt mixture, which may result in premature damages and increase of the life cycle cost of asphalt pavement. The service performances of asphalt pavement (e.g., high-

* Corresponding author at: School of Transportation Science and Engineering, Harbin Institute of Technology, Harbin 150090, China.
E-mail addresses: zhangchaonature@163.com (C. Zhang), tanyiqiu@hit.edu.cn (Y. Tan).

https://doi.org/10.1016/j.trd.2022.103395

Available online 23 July 2022

temperature rutting, low-temperature cracking and fatigue damage) are all affected by climate change (Knott et al., 2019; Qiao et al., 2015; Stoner et al., 2019). Rutting has been found as the most seriously affected performance (Gudipudi et al., 2017; Mills et al., 2009; Qiao et al., 2013).

Existing studies generally focused on the indexes of rutting depth and rutting life when reaching the design life and depth threshold, however, the continuous influence of climate change over the service life has been rarely considered. The influence of the future climate change on asphalt pavement rutting is expected to be not fixed, while it tends to increase with time. Thus, the conventional indexes cannot fully characterize the influence of climate change over the service life. Resilience analysis is a method of assessing the cumulative influences of disasters on systems, and resilience can be measured quantitatively by the accumulation of performance loss function over time (Li et al., 2020a; Martello et al., 2021; Sun and Zhang, 2020; Zhou and Chen, 2020). Resilience assessment has been widely used to assess the influences of various disasters on different infrastructures (Castillo et al., 2022; Nivedya et al., 2020; Ouyang and Duenas-Osorio, 2014), whereas it has not been applied in asphalt pavement research under climate change.

This paper aims to develop a resilience assessment method to comprehensively assess the influence of climate change on asphalt pavement rutting over the service life. In addition, several Chinese representative cities are taken as examples since there have been rare researches on asphalt pavement under future climate change in China. First, the original resilience method is extended to fit the system whose performance level continues to decline. Then, the calculation formulas of rutting resilience are derived by combining the rutting prediction model and the level assessment model based on the extended resilience method. Subsequently, the influences of climate change on asphalt pavement rutting in representative cities in China are studied using the proposed resilience index.

2. Resilience methodology

2.1. Resilience concept

Resilience theory can be adopted to comprehensively assess the influence of disasters on system performance over the service life. The performance response function (PRF) method has been extensively used to quantitatively assess the resilience (Ouyang et al., 2012; Xiao et al., 2022). Fig. 1 depicts two time-dependent curves, including $P_T(t)$ and $P_R(t)$. $P_T(t)$ curve represents the PRF curve without disaster, which can be modeled as a constant; $P_R(t)$ curve is the PRF curve with disaster, which is the result of the joint action of disaster and the resistance ability and recovery ability of the system. The performance response process can be assigned into three stages (Fig. 1), including the damage stage ($t_0 < t \leq t_1$), the disturbance steady stage ($t_1 < t \leq t_2$), and the recovery stage ($t_2 < t \leq t_3$).

As shown in Fig. 1, a disaster occurs at t_0, and then the performance level decreases from 100% (corresponding to the level without disaster) to a certain level (P_1) at t_1; when $t_1 < t \leq t_2$, the performance level of the system is kept at P_1; at the time of t_2, the disaster ends and the performance level starts to recover; the performance level returns to the initial state at t_3. The value of P_1 ranges from 0 to 100%. Next, resilience indexes can be generally quantified as the areas enclosed by the two curves and x-axis. The area enclosed by $P_R(t)$ and x-axis from t_0 to t_3 is referred to as resilience residual (Fig. 1), and the area enclosed by $P_T(t)$ and $P_R(t)$ can be referred to as resilience loss, which are expressed by Eq. (1) and (2), respectively.

$$RR = \int_{t_0}^{t_3} P_R(t)dt \tag{1}$$

$$RL = \int_{t_0}^{t_3} (P_T(t) - P_R(t))dt \tag{2}$$

Where RR denotes the resilience residual; RL represents the resilience loss. Notably, smaller RL or larger RR implies higher resilience.

2.2. Resilience of resistance stage and recovery stage

In general, resilience is capable of assessing the resistance ability of the system under disasters and the recovery ability after disasters. The performance response of the system at the damage stage and disturbance steady stage can both reflect the ability of the

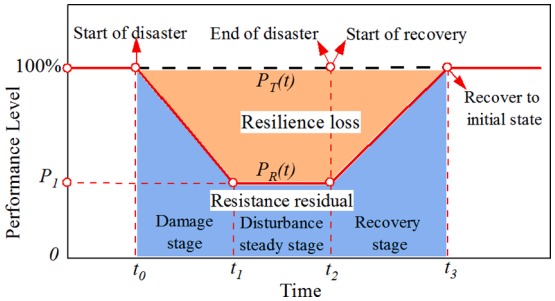

Fig. 1. Typical PRF curve with disaster.

system to resist disasters, therefore, the damage stage and disturbance steady stage can be both included in the resistance stage. In accordance with the different stages of disaster impact, resilience loss (*RL*) can be assigned into two parts as shown in Fig. 2, which are expressed by Eq. (3) and (4), respectively.

$$RS = \int_{t_0}^{t_1} (P_T(t) - P_R(t))dt \tag{3}$$

$$RC = \int_{t_1}^{t_3} (P_T(t) - P_R(t))dt \tag{4}$$

Where *RS* represents the resilience loss of resistance stage; *RC* denotes the resilience loss of recovery stage (Fig. 2). Notably, both smaller *RS* and smaller *RC* imply higher resilience.

2.3. Recovery strategies and recovery patterns

The recovery methods is divided into artificial recovery and natural recovery in accordance with the different driving factors in the system recovery process, i.e., whether there are anthropogenic factors involved. Further, according to the different combinations of the two recovery methods, there are four recovery strategies as depicted in Fig. 3. Natural recovery comprises the elastic recovery of the system (e.g., spring), and the recovery caused by natural environmental factors (e.g., wind and, sunshine).

Based on the different recovery results of system performance, the PRF curves can be summarized into six patterns as presented in Fig. 4.

Pattern 1 - the system performance after the disaster exceeds the initial level, which generally requires the participation of artificial recovery (Aros-Vera et al., 2021; Francis and Bekera, 2014).

Pattern 2 - the system performance is completely recovered to the initial level, which is the most common form in resilience researches (Manrique-Alba et al., 2022; Zhang et al., 2021c).

Pattern 3 - the system is damaged in the disaster, and the performance is partially recovered after the disaster, which is lower than the initial level (Aros-Vera et al., 2021; Zhou and Chen, 2020).

Pattern 4 - the system performance decreases in the disaster, and remains at a low level after the disaster without natural recovery and artificial recovery.

Pattern 5 - The system is completely destroyed in the disaster, and not rebuilt after the disaster.

Pattern 6 - the system performance decreases in the disaster, and it decreases continuously after the disaster.

For system with the capability of natural recovery, the performance can be fully recovered to the initial level or partially recovered to a lower level after the disaster (patterns 2 and 3), and generally will not exceed the initial level (pattern 1). For system without natural recovery, the performance can be recovered with the participation of artificial recovery. For example, electric power system and water supply system are vital urban infrastructures, and their performance levels will decrease under the action of earthquake. In practice, different degrees of manual repair after the earthquake will lead to different recovery results of the system (patterns 1–3). The system may be directly destroyed (pattern 5) when subjected to high-grade earthquake. If the pipeline of the water supply system has cracks and leaks in the earthquake, and is not well repaired after the earthquake, the cracks may increase continuously, and the performance of the water supply system will continue to decline (pattern 6).

2.4. Resilience assessment for resistance stage

In fact, the performances of all man-made systems can be recovered to a certain extent with the participation of artificial recovery after disasters. Even if the system is destroyed in a disaster, its performance can be completely recovered through artificial reconstruction. Thus, any man-made system is able to recover its performance.

In general, the disasters encountered by systems in current resilience researches are short-term strong disasters (e.g., earthquake, hurricane, and flood) (Abdelhady et al., 2020; Hasanzad and Rastegar, 2022; Sen et al., 2022), and the system performances will be

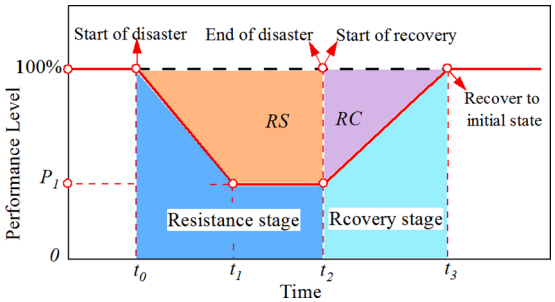

Fig. 2. Resilience of resistance stage and recovery stage.

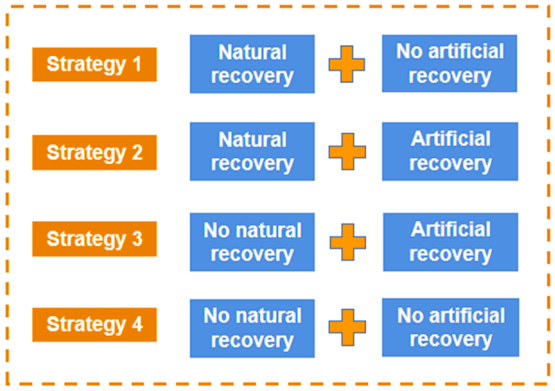

Fig. 3. Recovery strategies of systems.

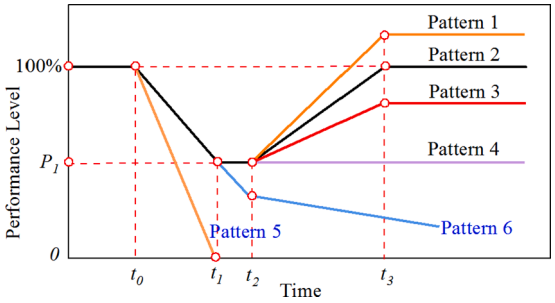

Fig. 4. PRF curves of different recovery patterns.

recovered under natural or anthropogenic factors after the disaster. However, system performance may tend to decrease under persistent climate stressors (patterns 5 and 6 in Fig. 4). For example, the rutting level of asphalt pavement gradually decreases under the repeated load of vehicles, and the strength of reinforced concrete piers tends to decline with the continuous corrosion of chloride ions in seawater. In fact, previous studies have mentioned patterns 5 and 6 in resilience researches (Fig. 4), but there is no in-depth study on them (Nipa and Kermanshachi, 2022; Xiao et al., 2022).

Without artificial recovery, the performance of system 1 (Figs. 5 and 6) will decrease continuously under long-term persistent disaster during the service period from t_{10} to t_{30}. There are two ways to improve the resilience of the above system over the service period, which is to improve the system performance through artificial recovery during the service period (system 2 in Fig. 5), or improve the resilience potential of the system during design and construction (system 3 in Fig. 6). If the system is repaired or rebuilt at t_{20}, the performance level can be improved from P_1 to 100% in a short time (system 2 in Fig. 5). The performance level of system 3 decreases more slowly than that of system 1 (Fig. 6), suggesting that system 3 has higher resistance throughout its service life.

For systems 1 and 3 in Fig. 6, the resilience loss of recovery stage (RC) is zero, and the loss resilience of resistance stage (RS) is equal to loss resilience (RL) (Fig. 2). Resilience assessment of resistance stage can be considered part of the general resilience analysis, or a method to assess the system resilience whose performance level continues to decline.

Rutting is the permanent deformation of asphalt pavement surface at the wheel track due to ambient temperature and vehicle load (Daniel, 2017; Zhang et al., 2021a; Zhang et al., 2017). With the increase of the service life, the rutting depth will increase

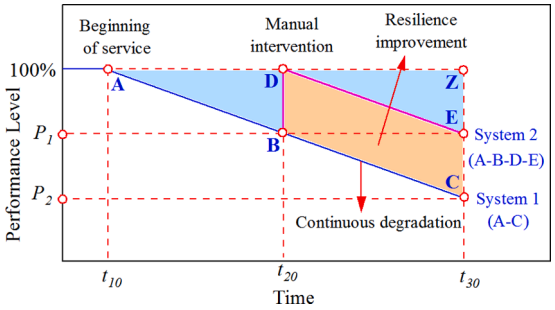

Fig. 5. Improvement of resilience with manual intervention.

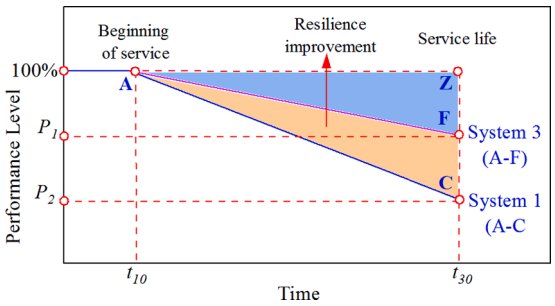

Fig. 6. Improvement of resilience of resistance stage.

continuously, while the rutting level index tends to decrease from 100% (systems 1 and 3 in Fig. 6). Therefore, Resilience assessment of resistance stage is suitable for rutting over the service life of asphalt pavement.

3. Resilience assessment for rutting

3.1. Effective temperature under climate change

The effective temperature is often used as a constant in the rutting design of asphalt pavement (El-Basyouny and Jeong, 2009; Jitsangiam et al., 2022; Li et al., 2017), which can be obtained in accordance with air temperature by Eq. (5) and (6) in China.

$$T_k = T_i + 0.016h \tag{5}$$

$$T_i = 1.04T_n + 0.22(T_h - T_c) \tag{6}$$

Where T_i represents the basic annual effective temperature (°C); T_k denotes the annual effective temperature considering the thickness of asphalt mixture layer (°C); T_n expresses annual average temperature in the region (°C); T_h is the average temperatures of the hottest month (T_h); T_c is the average temperatures of the coldest month (°C); h denotes the thickness of asphalt mixture layer (mm), which is commonly 180 mm in China for high-grade asphalt pavement.

The effective temperatures of 629 meteorological stations in China are obtained by Eq. (5) and (6). The historical meteorological data are used to calculate the effective temperatures before 2020, while the predicted temperature under RCP4.5 and RCP8.5 are used to calculate the effective temperatures after 2020. Fig. 7 presents the overall trends of temperature change in China from 1965 to 2098.

The CMIP5 set of experiments consists of projection experiments of the 21st century climate and simulations of 20th century climate (historical experiments) under the new greenhouse gas emission scenarios termed Representative Concentration Pathways (RCP) (Chong-Hai and Ying, 2012; Underwood, 2021; Wang and Chen, 2014). RCP4.5 pathway can stabilize radiative forcing at 4.5 W/m^2 in 2100, and RCP8.5 can simulate adapted emissions with stabilizing close to 8.5 W/m^2 (Ji and Kang, 2013; Lee et al., 2014). RCP4.5 scenario is considered to be a relatively optimistic scenario for effective control of greenhouse gas emissions, while RCP8.5 scenario indicates the consequences of failure to reduce greenhouse gas emissions in accordance with global agreements.

Five CMIP5 models with wide applications in China are adopted, including HadGEM2-ES, CSIRO-Mk3-6-0, NESM1-M, EC-EARTH, as well as MPI-ESM-MR. The predicted temperature data applied are the averages of the five models. As depicted in Fig. 7, the effective temperatures will increase continuously under RCP4.5 and RCP8.5 by the end of this century. The growth rates of effective temperature under RCP8.5 gradually increase, whereas these rates tend to decrease under RCP4.5.

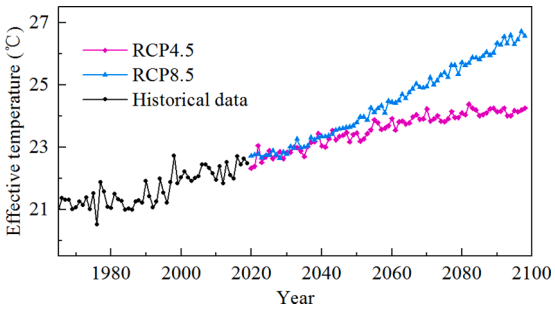

Fig. 7. Average effective temperatures for asphalt pavement rutting in China.

3.2. Rutting depth under climate change

In general, design temperature (T_0) for asphalt pavement is the average value of the annual effective temperatures (T_k) over the past three decades as shown in Eq. (7), and the corresponding year range [Ya, Yb] is referred to as design time. Similarly, service temperature (T_s) is the average value of the effective temperatures (T_k) during the service life as shown in Eq. (8), and the corresponding year range [Yc, Yd] is referred to as service time.

$$T_0 = \frac{1}{Yb - Ya + 1} \sum_{k=Ya}^{Yb} T_k \tag{7}$$

$$T_s = \frac{1}{Yd - Yc + 1} \sum_{k=Yc}^{Yd} T_k \tag{8}$$

To compare the influences of climate change in different cities, there is an assumption that, the rutting depth just reaches the design threshold (RD_0) when the loading cycle reaches the design traffic volume (N_0) without considering the climate change (Fig. 8). According to the specifications for design of highway asphalt pavement in China, there is a correlation as expressed in Eq. (9).

$$RD_0 = K_0 T_0^{2.93} N_0^{0.48} \tag{9}$$

Where RD_0 is the design threshold of rutting depth (mm); N_0 denotes the design traffic volume (loading cycle), which is the total predicted equivalent traffic volume over the service life; K_0 represents the comprehensive structure coefficient, a parameter correlated with pavement structure and material performance. The design threshold refers to the maximum rutting depth allowed in the pavement design, and it is generally 15 mm for high-grade asphalt pavement in China.

Because of the increase of the effective temperature (T_k) under climate change (Fig. 7), the service temperature (T_s) will be higher than the design temperature (T_0). The actual rutting depth (RD_s) considering the climate change when reaching the design traffic volume (N_0) can be calculated as Eq. (10). It is obvious that RDs exceeds RD_0 (Fig. 8).

$$RD_s = RD_0 \left(\frac{T_s}{T_0}\right)^{2.93} \tag{10}$$

The rutting depth (RD) considering the climate change at loading cycle N ($N \le N_0$) can be written as Eq. (11).

$$RD = RD_0 \left(\frac{T_s}{T_0}\right)^{2.93} \left(\frac{N}{N_0}\right)^{0.48} \tag{11}$$

3.3. Performance level curve for rutting

To apply the resilience method in rutting assessment, the rutting depth-loading cycle curve should be translated to the rutting level-service time curve. In accordance with highway performance assessment standards in China (2018), there is a correlation between rutting depth and rutting level (RI), which is written in Eq. (11).

$$RI(RD) = \begin{cases} 100 - a_0 RD (RD \le RD_a) \\ 90 - a_1 \times (RD - RD_a) (RD_a < RD \le RD_b) \\ 0 (RD > RD_b) \end{cases} \tag{11}$$

Where RD_a and RD_b denote the rutting depth parameters, taken as 10 mm and 40 mm, respectively; a_0 and a_1 represent the model parameters, taken as 1 and 3, respectively.

By combining Eq. (10) and (11), the correlation between rutting level and loading cycle can be obtained as Eq. (12).

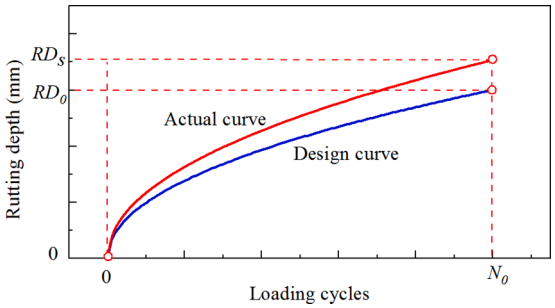

Fig. 8. Rutting depth curves with loading cycles.

$$RI(N)=\begin{cases}100-RD_0\left(\frac{T_s}{T_0}\right)^{2.93}\left(\frac{N}{N_0}\right)^{0.48} & (N\le N_a)\\ 120-3RD_0\left(\frac{T_s}{T_0}\right)^{2.93}\left(\frac{N}{N_0}\right)^{0.48} & (N_a<N\le N_b)\\ 0 & (N>N_b)\end{cases} \tag{12}$$

The loading cycle (N) corresponding to rutting depth (RD) is expressed as Eq. (13). By replacing RD_a and RD_b with RD, the corresponding load cycles N_a and N_b can be derived.

$$N=\left(\frac{RD}{RD_0}\right)^{2.08}\left(\frac{T_0}{T_s}\right)^{6.1}N_0 \tag{13}$$

Traffic volume prediction generally adopts the form of equal ratio series, and the design traffic volume (N_0) during service life can be calculated as Eq. (14).

$$N_0=N_1\frac{q^{t_0}-1}{q-1} \tag{14}$$

Where t_0 is the designed service life (year), which is generally 15 years for high-grade asphalt pavement in China; N_1 is the traffic volume in the first year; q is the average growth rate of annual traffic volume, and should be determined according to the traffic survey. In addition, to compare the influences of climate change in different cities, q is taken as 1.05 in the following resilience calculation.

According to Eq. (14), the cumulative traffic volume (N) at service time (t) is expressed as Eq. (15).

$$N=N_1\frac{q^t-1}{q-1}=N_0\frac{q^t-1}{q^{t_0}-1} \tag{15}$$

By combining Eq. (12) and (15), the correlation between rutting level and service life can be obtained as Eq. (16).

$$RI(t)=\begin{cases}100-RD_0\left(\frac{T_s}{T_0}\right)^{2.93}\left(\frac{q^t-1}{q^{t_0}-1}\right)^{0.48} & (t\le t_a)\\ 120-3RD_0\left(\frac{T_s}{T_0}\right)^{2.93}\left(\frac{q^t-1}{q^{t_0}-1}\right)^{0.48} & (t_a<t\le t_b)\\ 0 & (t>t_b)\end{cases} \tag{16}$$

The service life (t) corresponding to rutting depth (RD) is expressed as Eq. (17). By replacing RD_a and RD_b with RD, the corresponding service life t_a and t_b can be derived.

$$t=log_q\left(\left(\frac{RD}{RD_0}\right)^{2.08}\left(\frac{T_0}{T_s}\right)^{6.1}(q^{t_0}-1)+1\right) \tag{17}$$

The design curve and actual curve of rutting level over the service life can be obtained by Eq. (16) and (17) as presented in Fig. 9. It is obvious that the actual rutting level considering the climate change is generally lower than the design level.

3.4. Resilience assessment

Eq. (18) shows that the resilience residual based on rutting level is expressed as:

$$RR=\int_0^{t_0}RI(t)dt=\int_0^{t_a}RI(t)dt+\int_{t_a}^{t_b}RI(t)dt+\int_{t_b}^{t_0}RI(t)dt \tag{18}$$

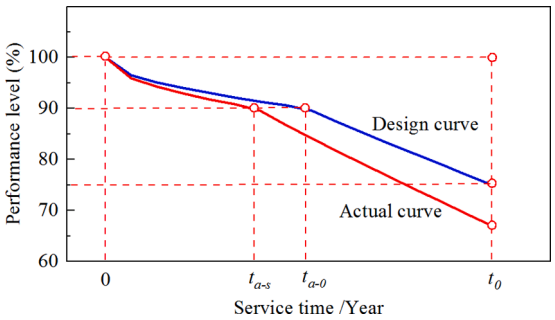

Fig. 9. Rutting level curve over service life.

Eq. (11) shows that when $t > t_b$, $RI = 0$. Accordingly, the upper limit value of integration in Eq. 11 can be the smaller of t_0 and t_b, i.e., set $t_p = \min(t_0, t_b)$. Subsequently, Eq. (18) is simplified as Eq. (19).

$$RR = \int_0^{t_a} RI(t)dt + \int_{t_a}^{t_p} RI(t)dt \tag{19}$$

Eq. (20) is derived by substituting Eq. (16) into Eq. (19).

$$\mathrm{RR} = 120t_0 - 20t_a - \frac{RD_0}{(q^{t_0}-1)^{0.48}}\left(\frac{T_s}{T_0}\right)^{2.93}\left(\int_0^{t_p}(q^t-1)^{0.48}dt + 2\int_{t_a}^{t_p}(q^t-1)^{0.48}dt\right) \tag{20}$$

The relative resilience residual (R_r) is calculated by Eq. (21).

$$\begin{aligned} R_r &= \frac{RR}{100t_0} \\ &= 1.2 - \frac{t_a}{5t_0} - \frac{RD_0}{100t_0(q^{t_0}-1)^{0.48}}\left(\frac{T_s}{T_0}\right)^{2.93}\left(\int_0^{t_p}(q^t-1)^{0.48}dt + 2\int_{t_a}^{t_p}(q^t-1)^{0.48}dt\right) \end{aligned} \tag{21}$$

Next, the relative resilience loss (R_l) can be calculated by Eq. (22).

$$\begin{aligned} R_l &= 1 - R_r \\ &= \frac{t_{as}}{5t_0} - 0.2 + \frac{RD_0}{100t_0(q^{t_0}-1)^{0.48}}\left(\frac{T_s}{T_0}\right)^{2.93}\left(\int_0^{t_p}(q^t-1)^{0.48}dt + 2\int_{t_{as}}^{t_p}(q^t-1)^{0.48}dt\right) \end{aligned} \tag{22}$$

When climate change is not considered, the service temperature (T_S) is equal to the design temperature (T_0). According to Eq. (22), the relative resilience residual without considering climate change (R_{l0}) is expressed as Eq. (23).

$$R_{l0} = \frac{t_{a0}}{5t_0} - 0.2 + \frac{RD_0}{100t_0(q^{t_0}-1)^{0.48}}\left(\int_0^{t_p}(q^t-1)^{0.48}dt + 2\int_{t_{a0}}^{t_p}(q^t-1)^{0.48}dt\right) \tag{23}$$

The influence degree (d) of climate change on rutting resilience can be calculated by Eq. (24).

$$d = \frac{R_l - R_{l0}}{R_{l0}} \tag{24}$$

4. Influence of climate change based on rutting resilience

4.1. Key parameters of resilience assessment

Eq. (24) shows that the influence degree of climate change is primarily dependent on T_s and T_0. The correlation between T_s and T_0 is written as:

$$T_s = T_0 + \frac{v\Delta t}{10} \tag{25}$$

$$\Delta t = \frac{Yd + Yc}{2} - \frac{Yb + Ya}{2} \tag{26}$$

Where v denotes the average growth rate (°C/10a) of effective temperature from the beginning of design time (Ya) to the end of service time (Yd). The unit (°C/10a) means degrees celsius every ten years, and it is usually employed in meteorology researches (Chong-Hai and Ying, 2012). Δt denotes the lag time (year) of design time [Ya, Yb] relative to service time [Yc, Yd].

In general, the recommended design temperatures (T_0) in the specifications for design of highway asphalt pavement (SDHAP) in China are calculated based on the meteorological data over the past 30 years before release of the specifications. The specifications are generally implemented for 10 years, and the designed service life of high-grade asphalt pavement in China is 15 years. Therefore, the lag time (Δt) ranges from 22.5 to 32.5 years.

The latest version of the SDHAP is released in 2017, and the design specification is assumed to be updated every ten years. To study the influences of climate change in the near, medium and long terms of this century, three versions of SDHAP in 2017, 2047 and 2077

Table 1
Percentile values of design temperature and growth rate.

Percentile	Minimum	25%	50%	75%	Maximum
T_0 (°C)	3.0	18.8	23.4	26.7	33.2
v (°C/10 year)	0.10	0.27	0.34	0.46	0.87

are selected for analysis, with the corresponding design times of 1987–2016, 2017–2046, and 2047–2076, respectively. When the asphalt pavements are put into service in the fifth year of the specification implementation, the corresponding service times are 2022–2036, 2052–2066, and 2082–2096, respectively.

For 629 meteorological stations distributed throughout China, design temperature (T_0) and growth rate (v) in the corresponding periods are calculated, and the percentile values are listed in Table 1.

Based on Eq. (24) and Table 1, the influence degrees of growth rate (T_0) and design temperature (v) on rutting resilience can be obtained as depicted in Figs. 10 and 11, respectively. With the increase of the growth rate, the influence degrees show a nearly linear growth trend (Fig. 9). For the pavement at the design temperature of 23.4 °C, the influence degree of the growth rate of 0.46 °C/10 year is 77.9% higher than that of 0.27 °C/10a. The influence degree is reduced with the increase of the design temperature, and the reduction rate is higher before 15 °C and lower after 15 °C (Fig. 10).For the pavement with a growth rate of 0.46 °C/10a, the influence degree of the design temperature of 26.7 °C is 15.7% lower than that of 18.8 °C.

4.2. Temperature parameters of representative cities

Because China is located in the northern hemisphere of the earth, and latitude is the most important factor affecting temperature, the temperatures in China tend to increase from north to south on the whole. Eight representative cities from north to south in eastern China are selected to investigate the influences of climate change. Mohe (MH), Harbin (HRB), Beijing (BJ), Zhengzhou (ZZ), Wuhan (WH), Changsha (CS), Guangzhou (GZ) and Haikou (HK) are marked in the map of China as shown in Fig. 12.

Figs. 13 and 14 depict the design temperatures (T_0) of the representative cities in different periods under different RCP scenarios. Under both RCP4.5 and RCP8.5, the design temperatures tend to increase from north to south. Over time, the design temperatures tend to increase as well. To be specific, the design temperatures of Mohe and Harbin in Northeast China are significantly lower than those of other cities.

Figs. 15 and 16 show the growth rates (v) of effective temperature of the representative cities in different periods under different scenarios. The growth rates from north to south do not significantly change under the two RCP scenarios. Over time, the growth rates tend to decrease under RCP4.5 while increasing under RCP8.5. Furthermore, the growth rate of Zhengzhou for 1987–2036 period under RCP4.5 is significantly higher than those of other cities.

4.3. Resilience assessment under climate change

The influence degrees (d) of climate change on representative cities based on resilience assessment are obtained by Eq. (22) - (24), as depicted in Figs. 17 and 18. 2052RCP4.5 in the legend means that the road is in service from 2052, with the design time from 2017 to 2046 and the service life from 2052 to 2066. The influence degrees tend to decrease from north to south under both RCP4.5 and RCP8.5, showing a change trend opposite to the design temperatures (T_0). For 2022RCP4.5 and 2082RCP8.5, the influence degrees of climate change in the northernmost city (Mohe) are both more than 4 times of those in the southernmost city (Haikou).

The growth rates (v) of Harbin and Beijing are relatively close, while the influence degrees of Harbin are significantly higher than those of Beijing. The reason for the above result is that the design temperatures (T_0) of the former are significantly lower than those of the latter. Interestingly, the influence degrees of Zhengzhou and Harbin are close for 2022RCP4.5. This is because the growth rates of Zhengzhou (0.446 °C/10a) is significantly higher than that of Harbin (0.335 °C/10a) though the design temperature of Zhengzhou (24.6 °C) is noticeably higher than that of Harbin (17.3 °C).

Over time, the influence degrees tend to decrease under RCP4.5 while increasing under RCP8.5, consistent with the change trends of the growth rates. In Mohe, the influence degree decreases rapidly from 0.501 to 0.382, and then it further decreases to 0.199 over time. However, the influence degrees in Guangzhou and Haikou under 2022RCP4.5 are lower than those under 2052RCP4.5 since the growth rates of the former are significantly lower than those of the latter. Growth rates are the main factors for the influence degrees in cities with high design temperatures (Guangzhou and Haikou).

The influence degrees under RCP4.5 are significantly higher than those under RCP8.5, and the differences of influence degrees between the two scenarios increase over time. For instance, in Heihe, the influence degree of RCP8.5 is 1.1 times that of RCP4.5 in

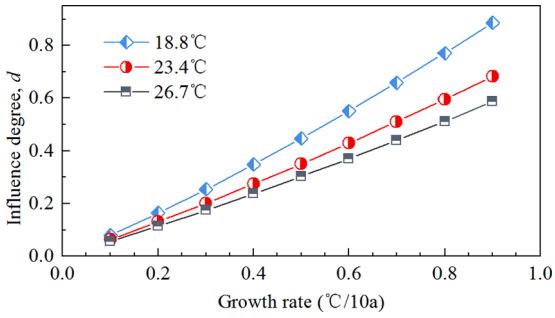

Fig. 10. Influence degrees with growth rate.

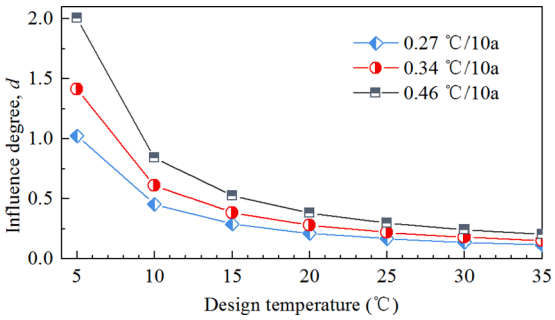

Fig. 11. Influence degrees with design temperature.

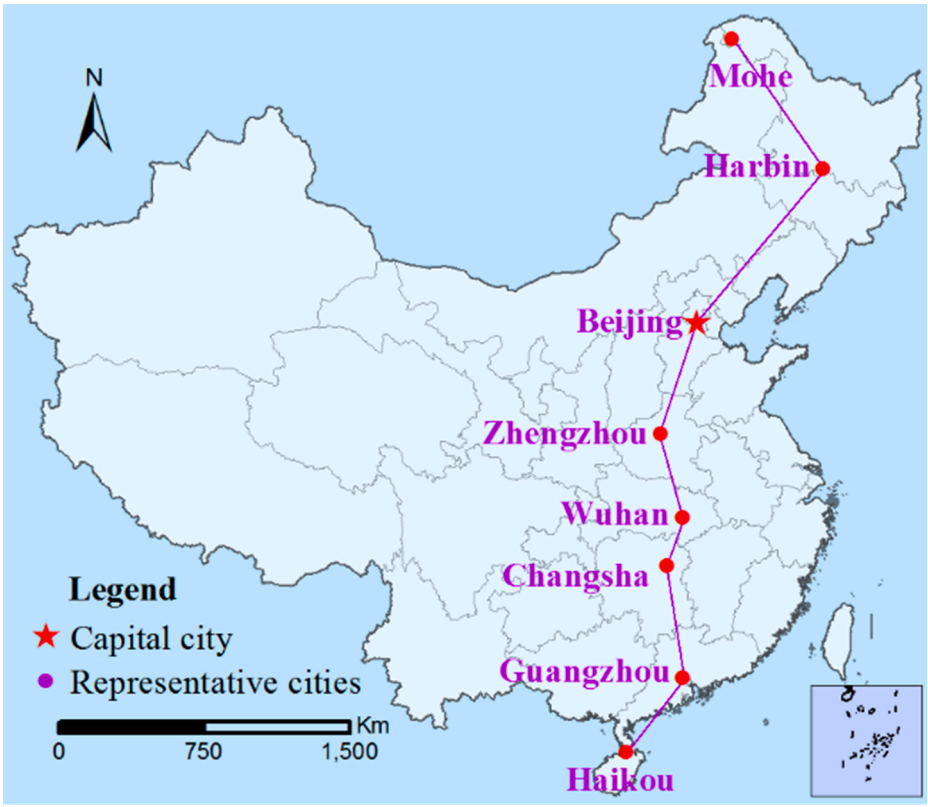

Fig. 12. Locations of representative cities in China.

2022, then increases to 2.3 times in 2052, and finally increases to 5.1 times in 2082 rapidly. In Haikou, the influence degree of RCP8.5 is 1.2 times that of RCP4.5 in 2022, then increases to 1.5 times in 2052, and finally increases to 3.4 times in 2082 rapidly. The examples of Heihe and Haikou suggest that, the influences of differences between the two scenarios are more significant in northern cities than those in southern cities.

5. Conclusions

This paper aims to develop a resilience assessment method to comprehensively assess the influence of climate change on asphalt pavement rutting over the service life. First, the original resilience method is extended to fit the system whose performance level continues to decline. Then, the calculation formulas of rutting resilience are derived by combining the rutting prediction model and the level assessment model based on the extended resilience method. Subsequently, the influences of climate change on asphalt pavement rutting in representative cities in China are explored using the proposed resilience index.

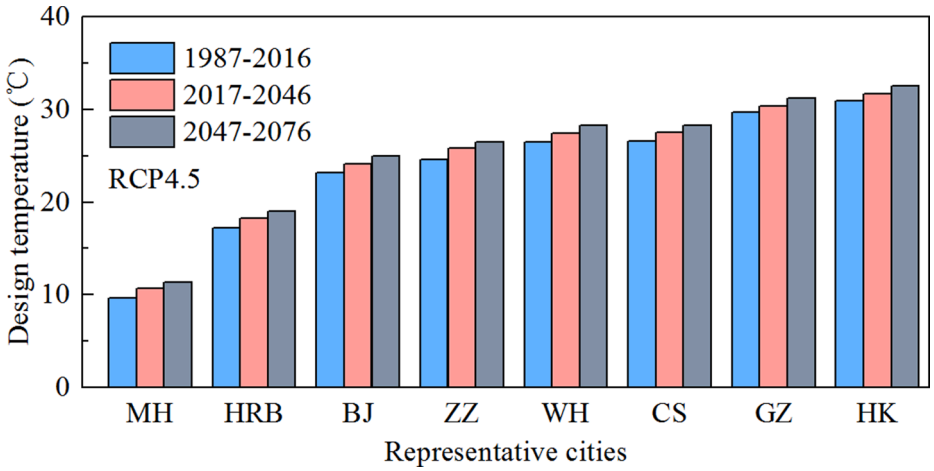

Fig. 13. Design temperatures under RCP4.5.

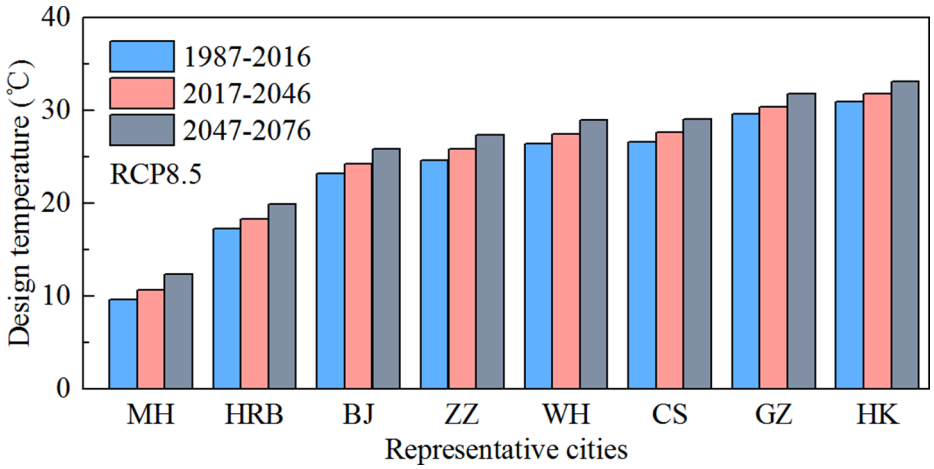

Fig. 14. Design temperatures under RCP8.5.

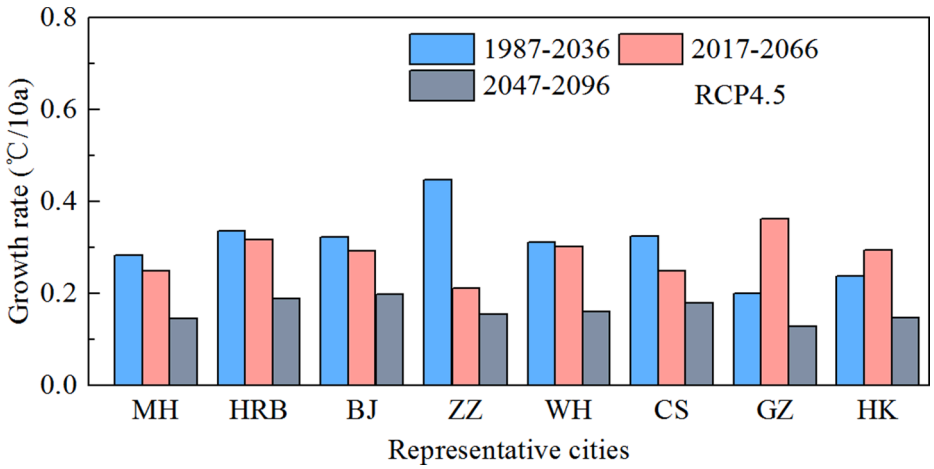

Fig. 15. Growth rates under RCP4.5.

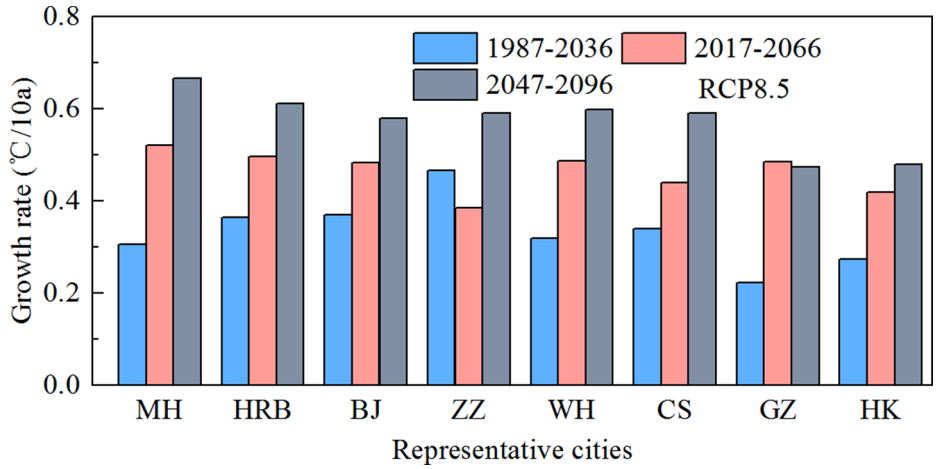

Fig. 16. Growth rates under RCP8.5.

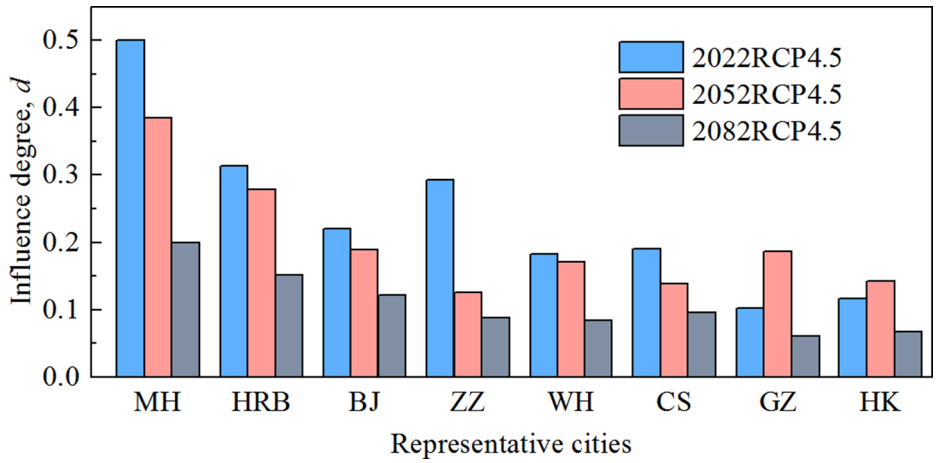

Fig. 17. Influence degree under RCP4.5.

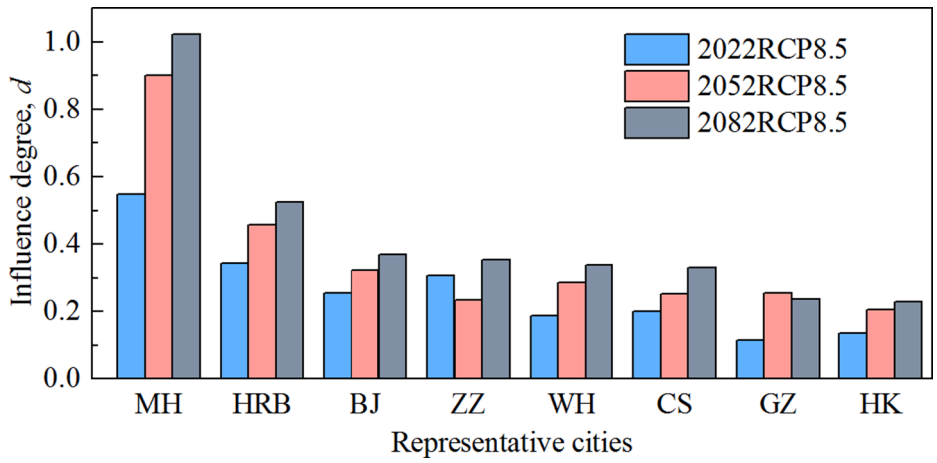

Fig. 18. Influence degree under RCP8.5.

(1) Resilience assessment can be conducted to comprehensively assess the influence of climate change on asphalt pavement rutting over the service life of asphalt pavement. In accordance with the different stages of disaster impact, system resilience can be generally separated into resilience of resistance stage and resilience of recovery stage, and resilience assessment for resistance stage is suitable for asphalt pavement rutting. The calculation formulas of rutting resilience are obtained by combining the rutting prediction model and the rutting level assessment model.
(2) The influence degrees of resilience are primarily dependent on design temperature and the growth rate of effective temperature under climate change. With the increase of the growth rate, the influence degrees tend to increase nearly linearly. With the increase of the design temperature, the influence degrees are reduced, and the reduction rate is higher before 15 °C and lower after 15 °C.
(3) The rutting resilience of asphalt pavement is significantly influenced by climate change in China. From north to south, the influence degrees tend to decrease under both RCP4.5 and RCP8.5, showing a change trend opposite to the design temperatures. Over time, the influence degrees tend to decrease under RCP4.5 while increasing under RCP8.5, consistent with the change trends of the growth rates.
(4) Neglecting climate change in rutting design of asphalt pavement will lead to insufficient resilience, especially in northern China. The influence degrees of climate change under RCP8.5 are obviously higher than those under RCP4.5, so it is necessary to calculate the effective temperature for rutting design according to the predicted temperature under RCP8.5 during the expected service period of the asphalt pavement.

It is noteworthy that this paper aims to assess the influence of climate change on the service performance of asphalt pavement in the whole service life based on the resilience index. Since existing studies have shown that the influence of climate change on asphalt pavement rutting is significantly greater than those on fatigue and thermal crack, rutting is taken as an example to illustrate pavement resilience. The proposed resilience method is still applicable to fatigue and thermal crack, whereas there may be differences in specific resilience values and influence degrees.

Declaration of Competing Interest

The authors declare that they have no known competing financial interests or personal relationships that could have appeared to influence the work reported in this paper.

Data availability

Data will be made available on request.

Acknowledgments

The authors acknowledged the financial supports from National Natural Science Foundation of China (U20A20315), European Union's Horizon 2020 research and innovation programme under the Marie Sklodowska-Curie (101030767), and Open Research Fund Program of Guangdong Key Laboratory of Urban Informatics (SZU51029202005). The authors thank Han Zhenyu in National Climate Center of China Meteorological Administration and Zhou Botao in Nanjing University of Information Science and Technology for providing the meteorological data. The authors also thank Lv Dagang, Wang Xudong, Feng Yangzhi and Xie Guorui for their suggestions in the research process. Thanks to the anonymous reviewers for comments that have notably helped us improve the manuscript.

References

Abdelhady, A.U., Spence, S.M.J., McCormick, J., 2020. A framework for the probabilistic quantification of the resilience of communities to hurricane winds. J. Wind Eng. Ind. Aerodyn. 206, 104376. https://doi.org/10.1016/j.jweia.2020.104376.
Fuhaid, A.A., Lu, Q., Luo, S., 2018. Laboratory Evaluation of Biobased Epoxy Asphalt Binder for Asphalt Pavement. J. Mater. Civ. Eng. 30 (7) https://doi.org/10.1061/(ASCE)MT.1943-5533.0002383.
Aros-Vera, F., Gillian, S., Rehmar, A., Rehmar, L., 2021. Increasing the resilience of critical infrastructure networks through the strategic location of microgrids: A case study of Hurricane Maria in Puerto Rico. Int. J. Disaster Risk Reduct. 55, 102055. https://doi.org/10.1016/j.ijdrr.2021.102055.
Blaauw, S.A., Maina, J.W., Mturi, G.A.J., Visser, A.T., 2022. Flexible pavement performance and life cycle assessment incorporating climate change impacts. Transport. Res. Part D: Transp. Environ. 104, 103203. https://doi.org/10.1016/j.trd.2022.103203.
Castillo, J.G.S., Bruneau, M., Elhami-Khorasani, N., 2022. Functionality measures for quantification of building seismic resilience index. Eng. Struct. 253, 113800. https://doi.org/10.1016/j.engstruct.2021.113800.
Chen, X., Wang, H., Horton, R., DeFlorio, J., 2021. Life-cycle assessment of climate change impact on time-dependent carbon-footprint of asphalt pavement. Transport. Res. Part D-Transp. Environ. 91, 102697. https://doi.org/10.1016/j.trd.2021.102697.
Chong-Hai, X., Ying, X., 2012. The projection of temperature and precipitation over China under RCP scenarios using a CMIP5 multi-model ensemble. Atmos. Oceanic Sci. Lett. 5 (6), 527–533.
Daniel, J.S., 2017. Roadways in a rut. Nat. Clim. Change 7 (10), 694–695.
El-Basyouny, M., Jeong, M.G., 2009. Effective Temperature for Analysis of Permanent Deformation and Fatigue Distress on Asphalt Mixtures. Transp. Res. Rec. 2127 (1), 155–163.
Francis, R., Bekera, B., 2014. A metric and frameworks for resilience analysis of engineered and infrastructure systems. Reliab. Eng. Syst. Saf. 121, 90–103.
Gao, Y., Zhang, Y., Zhang, C., Liu, X., Jing, R., 2022. Quantifying oxygen diffusion in bitumen films using molecular dynamics simulations. Constr. Build. Mater. 331, 127325. https://doi.org/10.1016/j.conbuildmat.2022.127325.

Gao, Y., Zhang, Y., Yang, Y., Zhang, J., Gu, F., 2019. Molecular dynamics investigation of interfacial adhesion between oxidised bitumen and mineral surfaces. Appl. Surf. Sci. 479, 449–462.
Gudipudi, P.P., Underwood, B.S., Zalghout, A., 2017. Impact of climate change on pavement structural performance in the United States. Transport. Res. Part D-Transp. Environ. 57, 172–184.
Hasanzad, F., Rastegar, H., 2022. Application of optimal hardening for improving resilience of integrated power and natural gas system in case of earthquake. Reliab. Eng. Syst. Saf. 223, 108476. https://doi.org/10.1016/j.ress.2022.108476.
Ji, Z., Kang, S., 2013. Projection of snow cover changes over China under RCP scenarios. Clim. Dyn. 41 (3-4), 589–600.
Jitsangiam, P., Kumlai, S., Nikraz, H., 2022. New theoretical framework for temperature-effect integration into asphalt concrete pavement life prediction with respect to Australian pavement conditions. Road Mater. Pavement Des. 23 (3), 583–600.
Knott, J.F., Sias, J.E., Dave, E.V., Jacobs, J.M., 2019. Seasonal and Long-Term Changes to Pavement Life Caused by Rising Temperatures from Climate Change. Transp. Res. Rec. 2673 (6), 267–278.
Lee, J.-W., Hong, S.-Y., Chang, E.-C., Suh, M.-S., Kang, H.-S., 2014. Assessment of future climate change over East Asia due to the RCP scenarios downscaled by GRIMs-RMP. Clim. Dyn. 42 (3-4), 733–747.
Li, C., Fang, Q.i., Ding, L., Cho, Y.K., Chen, K.e., 2020a. Time-dependent resilience analysis of a road network in an extreme environment. Transport. Res. Part D: Transp. Environ. 85, 102395. https://doi.org/10.1016/j.trd.2020.102395.
Li, L., Gao, Y., Zhang, Y., 2020b. Crack length based healing characterisation of bitumen at different levels of cracking damage. J. Cleaner Prod. 258, 120709. https://doi.org/10.1016/j.jclepro.2020.120709.
Li, Q., Sheng, B., Huang, J., Li, C., Song, Z., Chao, L., Sun, W., Yang, Y., Jiao, B., Guo, Z., Liao, L., Li, X., Sun, C., Li, W., Huang, B., Dong, W., Jones, P., 2022. Different climate response persistence causes warming trend unevenness at continental scales. Nature. Clim. Change 12 (4), 343–349.
Li, Y.i., Liu, L., Xiao, F., Sun, L., 2017. Effective temperature for predicting permanent deformation of asphalt pavement. Constr. Build. Mater. 156, 871–879.
Lu, Q., Harvey, J.T., 2011. Laboratory Evaluation of Open-Graded Asphalt Mixes with Small Aggregates and Various Binders and Additives. Transp. Res. Rec. 2209 (1), 61–69.
Manrique-Alba, À., Beguería, S., Camarero, J.J., 2022. Camarero JJ. Sci. Total Environ. 810, 152374. https://doi.org/10.1016/j.scitotenv.2021.152374.
Martello, M.V., Whittle, A.J., Keenan, J.M., Salvucci, F.P., 2021. Evaluation of climate change resilience for Boston's rail rapid transit network. Transport. Res. Part D-Transp. Environ. 97, 102908. https://doi.org/10.1016/j.trd.2021.102908.
Meagher, W., Daniel, J.S., Jacobs, J., Linder, E., 2012. Method for Evaluating Implications of Climate Change for Design and Performance of Flexible Pavements. Transp. Res. Rec. 2305 (1), 111–120.
Mills, B.N., Tighe, S.L., Andrey, J., Smith, J.T., Huen, K., 2009. Climate Change Implications for Flexible Pavement Design and Performance in Southern Canada. J. Transp. Eng. 135 (10), 773–782.
Nipa, T.J., Kermanshachi, S., 2022. Resilience measurement in highway and roadway infrastructures: Experts' perspectives. Progress in Disaster. Science 14, 100230. https://doi.org/10.1016/j.pdisas.2022.100230.
Nivedya, M.K., Tao, M., Mallick, R.B., Daniel, J.S., Jacobs, J.M., 2020. A framework for the assessment of contribution of base layer performance towards resilience of flexible pavement to flooding. Int. J. Pavement Eng. 21 (10), 1223–1234.
Ouyang, M., Dueñas-Osorio, L., 2014. Multi-dimensional hurricane resilience assessment of electric power systems. Struct. Saf. 48, 15–24.
Ouyang, M., Dueñas-Osorio, L., Min, X., 2012. A three-stage resilience analysis framework for urban infrastructure systems. Struct. Saf. 36-37, 23–31.
Qiao, Y., Dawson, A.R., Parry, T., Flintsch, G.W., 2015. Evaluating the effects of climate change on road maintenance intervention strategies and Life-Cycle Costs. Transport. Res. Part D-Transp. Environ. 41, 492–503.
Qiao, Y., Flintsch, G.W., Dawson, A.R., Parry, T., 2013. Examining Effects of Climatic Factors on Flexible Pavement Performance and Service Life. Transp. Res. Rec. 2349 (1), 100–107.
Sanchis, I.V., Insa Franco, R., Martínez Fernández, P., Salvador Zuriaga, P., Font Torres, J.B., 2020. Risk of increasing temperature due to climate change on high-speed rail network in Spain. Transport. Res. Part D-Transp. Environ. 82, 102312. https://doi.org/10.1016/j.trd.2020.102312.
Sen, M.K., Dutta, S., Kabir, G., 2022. Modelling and quantification of time-varying flood resilience for housing infrastructure using dynamic Bayesian Network. J. Cleaner Prod. 361, 132266. https://doi.org/10.1016/j.jclepro.2022.132266.
Stoner, A.M.K., Daniel, J.S., Jacobs, J.M., Hayhoe, K., Scott-Fleming, I., 2019. Quantifying the Impact of Climate Change on Flexible Pavement Performance and Lifetime in the United States. Transp. Res. Rec. 2673 (1), 110–122.
Sun, J., Zhang, Z., 2020. A post-disaster resource allocation framework for improving resilience of interdependent infrastructure networks. Transport. Res. Part D-Transp. Environ. 85, 102455. https://doi.org/10.1016/j.trd.2020.102455.
Tollefson, J., 2021. Top climate scientists are sceptical that nations will rein in global warming. Nature 599 (7883), 22–24.
Underwood, B.S., 2021. A method to select general circulation models for pavement performance evaluation. Int. J. Pavement Eng. 22 (2), 134–146.
Underwood, B.S., Guido, Z., Gudipudi, P., Feinberg, Y., 2017. Increased costs to US pavement infrastructure from future temperature rise. Nature. Clim. Change 7 (10), 704–707.
Wang, F., Li, N.a., Hoff, I., Wu, S., Li, J., Maria Barbieri, D., Zhang, L., 2020a. Characteristics of VOCs generated during production and construction of an asphalt pavement. Transport. Res. Part D-Transp. Environ. 87, 102517. https://doi.org/10.1016/j.trd.2020.102517.
Wang, L., Chen, W., 2014. A CMIP5 multimodel projection of future temperature, precipitation, and climatological drought in China. Int. J. Climatol. 34 (6), 2059–2078.
Wang, T., Qu, Z., Yang, Z., Nichol, T., Clarke, G., Ge, Y.-E., 2020b. Climate change research on transportation systems: Climate risks, adaptation and planning. Transport. Res. Part D-Transp. Environ. 88, 102553. https://doi.org/10.1016/j.trd.2020.102553.
Wu, J., Han, Z., Xu, Y., Zhou, B., Gao, X., 2020. Changes in extreme climate events in China under 1.5 C–4 C global warming targets: Projections using an ensemble of regional climate model simulations. J. Geophys. Res.: Atmosph., 125, e2019JD031057.
Xiao, Y., Zhao, X., Wu, Y., Chen, Z., Gong, H., Zhu, L., Liu, Y., 2022. Seismic resilience assessment of urban interdependent lifeline networks. Reliab. Eng. Syst. Saf. 218, 108164. https://doi.org/10.1016/j.ress.2021.108164.
Yu, B., Lu, Q., 2012. Life cycle assessment of pavement: Methodology and case study. Transport. Res. Part D-Transp. Environ. 17 (5), 380–388.
Yu, B., Wang, S., Gu, X., Ni, F., Liu, Q., 2018. Environmental burden evaluation of hot in-place recycling of asphalt pavement based on discrete event simulation. Transport. Res. Part D-Transp. Environ. 65, 151–160.
Zhang, C., Tan, Y., Cyriaque, A.O., Han, M., Zhou, X., Meng, A., 2021a. A local fitting method to improve model calculation accuracy of flow point of asphalt mixture. Constr. Build. Mater. 268, 121178. https://doi.org/10.1016/j.conbuildmat.2020.121178.
Zhang, C., Tan, Y., Zhang, L., Li, G., Zhang, J., Wang, Y., 2021b. Developing fragility curves for asphalt mixture to assess the uncertainty of the permanent deformation performance. Constr. Build. Mater. 310, 125272. https://doi.org/10.1016/j.conbuildmat.2021.125272.
Zhang, J., Zhu, C., Li, X., Pei, J., Chen, J., 2017. Characterizing the three-stage rutting behavior of asphalt pavement with semi-rigid base by using UMAT in ABAQUS. Constr. Build. Mater. 140, 496–507.
Zhang, Y., Cai, B., Liu, Y., Jiang, Q., Li, W., Feng, Q., Liu, Y., Liu, G., 2021c. Resilience assessment approach of mechanical structure combining finite element models and dynamic Bayesian networks. Reliab. Eng. Syst. Saf. 216, 108043. https://doi.org/10.1016/j.ress.2021.108043.
Zhou, L., Chen, Z., 2020. Measuring the performance of airport resilience to severe weather events. Transport. Res. Part D-Transp. Environ. 83, 102362. https://doi.org/10.1016/j.trd.2020.102362.